Staging Liver Fibrosis with Hepatic Perivascular Adipose Tissue as a CT Biomarker

Skylar Chan[*1] SPENCER.CHAN@NIH.GOV
Tejas Sudharshan Mathai[*1] TEJAS.MATHAI@NIH.GOV
Praveen T.S. Balamuralikrishna[1] THOPPEYSRINIVP2@NIH.GOV
Vivek Batheja[1] VIVEK.BATHEJA@NIH.GOV
Jianfei Liu[1] JIANFEI.LIU@NIH.GOV
Meghan G. Lubner[2] MLUBNER@UWHEALTH.ORG
Perry J. Pickhardt[2] PPICKHARDT2@UWHEALTH.ORG
Ronald M. Summers[2] RMS@NIH.GOV
[1] *Radiology and Imaging Sciences, National Institutes of Health Clinical Center, USA*
[2] *Department of Radiology, University of Wisconsin School of Medicine & Public Health, USA*

Abstract

Cirrhosis is the 12^{th} leading cause of death in the US. There are several CT imaging signs of late fibrosis, such as redistribution of liver segment volume, increased liver nodularity, and periportal space widening. Timely intervention can reverse the progression of early hepatic fibrosis, but later stages are irreversible. We hypothesize that the perivascular adipose tissue (PVAT) around the portal vein arising from periportal space widening may also be predictive of liver fibrosis. In this work, a fully automated pipeline was developed to segment the liver, spleen, portal vein and its branches. The PVAT in the vicinity of the portal vein was identified. From these structures, CT imaging biomarkers (volume, attenuation, fat fraction) were computed. They were used to build uni- and multivariate logistic regression models for diagnosing advanced fibrosis and cirrhosis. The best multivariate model for cirrhosis achieved 93.3% AUC, 78.9% sensitivity, and 93.4% specificity. For advanced fibrosis, the multivariate model obtained 88.7% AUC, 84.2% sensitivity, and 73.7% specificity. The automated approach may be useful for population-based studies of metabolic disease and opportunistic screening.

Keywords: CT, Liver Fibrosis, Cirrhosis, Perivascular Adipose Tissue, Portal Vein, Hepatic Arteries

1. Introduction

In the US, ∼4.5 million adults are affected by chronic liver disease (Centers for Disease Control and Prevention, 2024). It can lead to chronic inflammation, liver fibrosis, and eventually cirrhosis (Ludwig et al., 2021), which is the 12^{th} leading cause of death in the US. Chronic hepatitis B/C viral infection, alcohol abuse, and metabolic dysfunction-associated steatohepatitis (e.g., due to obesity or diabetes) can cause fibrosis. Timely intervention can reverse early fibrosis, and thus it is necessary to distinguish later stages (advanced fibrosis and cirrhosis) from earlier stages of fibrosis.

Liver biopsy is the gold standard for staging fibrosis, but it is invasive and suffers from sampling error. Lab serum tests can be used, but they are insufficient and cannot replace

[*] Contributed equally

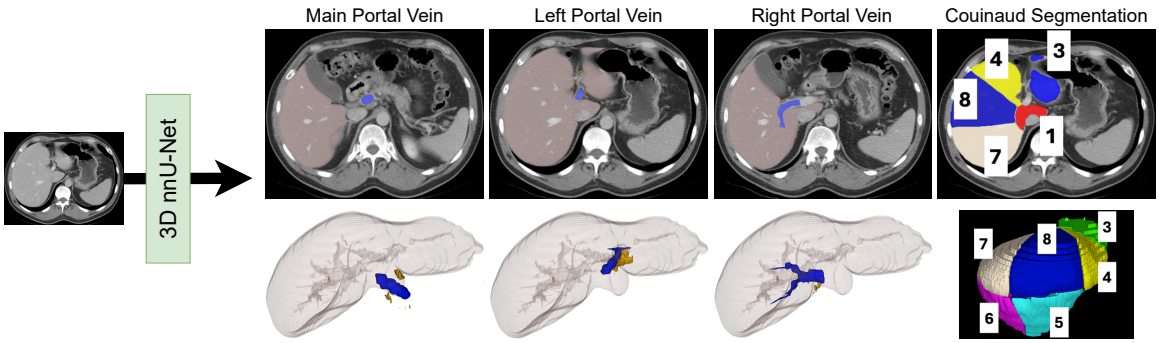

Figure 1: Automated framework for staging advanced fibrosis and cirrhosis. A 3D full resolution nnU-Net segmented the portal vein and its branches. Another model segmented the liver, Couinaud segments, and spleen. CT biomarkers (volume, attenuation, fat fraction) of the liver, spleen and perivascular adipose tissue (PVAT) were automatically derived. Liver (light brown), portal vein (blue), PVAT (yellow), and Couinaud segments (various colors).

histology (Pickhardt et al., 2016). Thus, non-invasive imaging-based biomarkers that perform better than biopsy or lab tests are sought (American Liver Foundation, 2022). Certain findings on abdominal contrast-enhanced CT (CECT) clearly indicate liver fibrosis, such as splenomegaly or ascites (Yin et al., 2021; Pickhardt et al., 2017), segmental redistribution (Lee et al., 2022), increased liver surface nodularity (Pickhardt et al., 2016; Mazumder et al., 2023; Mathai et al., 2024a,b; Lewis et al., 2024), and periportal space widening with cavernous transformation (Ludwig et al., 2021; Karcaaltincaba et al., 2007).

Periportal space widening is a manifestation of central liver atrophy (Ito et al., 2000). Due to an increase in distance between the main portal vein and the central liver (Ludwig et al., 2021), fat can expand into the periportal space. As the portal vein supplies 70-80% of hepatic blood flow (Ziessman et al., 2006), there may be local paracrine effects of fat accumulation on nearby regions (Kahn and Bergman, 2022). Recent works suggest that perivascular adipose tissue (PVAT), or the fat surrounding the blood vessels, can contribute to metabolic diseases via a distinct pathway (Kahn and Bergman, 2022; Valentini et al., 2023; Lastra and Manrique, 2015). However, there are very few studies investigating the relationship between fibrosis and PVAT accumulation around vessels feeding and draining the liver (Song et al., 2024; Ludwig et al., 2021; Ito et al., 2000).

In this paper, we hypothesize that PVAT biomarkers surrounding the portal vein in the liver can be used to stage fibrosis. To that end, a fully automated deep learning-based pipeline was developed to segment the liver, spleen, portal vein and its branches. PVAT and other CT imaging biomarkers were automatically computed. Uni- and multivariate models were built to differentiate advanced fibrosis and cirrhosis from earlier stages. To our knowledge, we are the first to introduce fine grained segmentations of the individual branches of the portal vein, and to quantitatively examine the utility of perivascular fat around the portal vein for staging liver fibrosis.

2. Methods

2.1. Patient Sample

In this retrospective study, three datasets containing abdominal contrast-enhanced CT (CECT) scans were used: (1) the public Medical Segmentation Decathlon (MSD) Hepatic Vessels dataset (Task-8) (Antonelli et al., 2022), (2) an internal National Institutes of Health (NIH) dataset, and (3) an external dataset from the University of Wisconsin (UW).

In the MSD training data subset, portal venous CT volumes from 157 patients (out of 303) were used. The CT volumes in which the portal vein was clearly visible for annotation were chosen. Each CT volume in the training data subset also contained the segmentations of liver tumors and hepatic vessels. Volume dimensions ranged from $512 \times 512 \times (26 - 177)$ voxels and the spacing ranged between (1.5 - 8) mm. The internal NIH dataset contained 43 patients with cirrhosis and other metabolic diseases having ascites (25 patients) and splenomegaly (18 patients) imaged at the NIH. CT volume dimensions ranged from $512 \times 512 \times (51 - 680)$ voxels and the spacing ranged between (1 - 5) mm.

In the external UW dataset, 480 patients (304 men, median age: 49 ± 9 years) underwent abdominal contrast-enhanced CT exams between 2000 – 2016 (Lee et al., 2022). The METAVIR staging system was used to categorize patients into 3 groups: patients who underwent CT imaging as potential kidney donors without any known symptoms of liver disease (F0, n = 151); patients with variable degrees of pre-cirrhotic hepatic fibrosis including early (F1, n = 52), intermediate (F2, n = 82), and advanced (F3, n = 56) fibrosis; and patients with chronic liver disease (cirrhosis) who had undergone evaluation for liver transplant (F4, n = 139). Within 1 year of the CT exam, a liver biopsy was required for patients in the early (F1), intermediate (F2), and advanced (F3) fibrosis cohorts.

Patients had the following causes of liver disease: chronic hepatitis B/C viral infection, alcoholism, biliary cirrhosis, sclerosing cholangitis and metabolic dysfunction-associated steatotic liver disease among others. Lab test results (FIB-4 and APRI scores) were also available. A variety of CT scanners were used (GE, Canon, and Siemens). The tube voltage ranged between 100 - 140 kVp with patient specific tube current settings. Volume dimensions ranged from $512 \times 512 \times (73 - 482)$ voxels and the spacing ranged between 2.5 - 5 mm.

2.2. Reference Standard

Liver tumors and hepatic vessels were available as a single label in the MSD dataset. First, the public TotalSegmentator (TS) tool (Wasserthal et al., 2023) was used to obtain liver and spleen segmentations in this dataset (157 volumes). Next, a public nnU-Net model trained on this dataset (Task-8) (Isensee et al., 2021) was run on the NIH dataset (43 volumes) to obtain the hepatic vessel tree. The model jointly segmented the the hepatic arteries, hepatic veins, and portal vein as a single label. Due to this, the portal vein and its branches (left and right) were manually annotated in the MSD and NIH datasets (200 volumes) by a research fellow. Two physicians (2+ years of experience) verified and corrected the segmentations of all structures (liver, spleen, portal vein and its left/right branches). The hepatic arteries and veins were separated from the portal vein annotation and treated as a separate label. This was due to the challenges in distinguishing the hepatic arteries and veins on CT.

For the external UW dataset, the eight Couinaud segments were obtained by a previously described tool (Lee et al., 2022). To evaluate the portal vein segmentation, five patients from each fibrosis stage were randomly chosen. The portal vein was manually segmented and verified by the same physicians in the 25 selected CT volumes.

2.3. Deep Learning Model

Fig. 1 shows the overall framework. The verified labels from the MSD and NIH datasets were used for training a 3D full-resolution nnU-Net. The model was tested on the external UW dataset. The labels were of the full liver, spleen, portal vein and its branches, and remaining vessels (hepatic arteries and vein). The nnU-Net model is the de facto standard for segmentation due to its award-winning performance on many tasks (Isensee et al., 2021), such as multi-organ segmentation in CT and MRI. It has often outperformed other architectures, such as transformers (Isensee et al., 2024). Thus, only the 3D nnU-Net model was used with no other comparative implementations. The rationale for this stemmed from the goal of this work, which is to extract a novel CT-based imaging biomarker (PVAT) and use it for diagnosing fibrosis.

The nnU-Net framework automatically determined a dataset "fingerprint", which included intensity normalization and resampling to a consistent spacing. Optimal hyperparameters were automatically computed and no changes were made to the default values. The following training parameters were set: 6 stages with 2 convolution layers per stage, feature maps per stage were [32, 64, 128, 256, 320, 320], kernel sizes were [1, 3, 3, 3, 3, 3], batch size of 2, learning rate of 0.01, SGD optimizer, and 1000 training epochs. The model learned to segment the target structures and iteratively refined the predictions during training via a loss function, which was a combination of the Dice loss and the binary cross entropy loss. Training was conducted on one NVIDIA A100-SXM4-40GB GPU. Segmentations of hepatic arteries and veins were not used at test time.

2.4. Automated Extraction of Imaging-based Biomarkers

Liver and Spleen Biomarkers: CT biomarkers were computed from nnU-Net segmentations of the liver and spleen in the UW dataset. Couinaud segments, Biomarkers These included: volume, attenuation (mean and std. dev.), liver segmental volume ratio (LSVR, the volume ratio of liver segments 1-3 to 4-8) (Lee et al., 2022), and liver surface nodularity (LSN) (Mathai et al., 2024a,b; Lewis et al., 2024).

PVAT Biomarkers: The portal vein segmentation was dilated with a kernel size of $4\times4\times4$ voxels following prior research (Nguyen et al., 2024; Chatterjee et al., 2022). Other kernel sizes ($3\times3\times3$, $5\times5\times5$) were also tested and no qualitative difference was found between them. As shown in Fig. 2, this dilated area represented the perivascular region. Voxels corresponding to PVAT in the perivascular region that fell within the HU range of $[-190, -30]$ were identified (Nguyen et al., 2024). Biomarkers were calculated from these PVAT voxels: volume, mean and std. dev. (SD) of CT attenuation, and fat fraction (ratio of the number of PVAT voxels to the number of perivascular region voxels). To account for variations in scanners, acquisition, and disease characteristics, the PVAT CT attenuation was normalized by the average vessel lumen attenuation (Chatterjee et al., 2022).

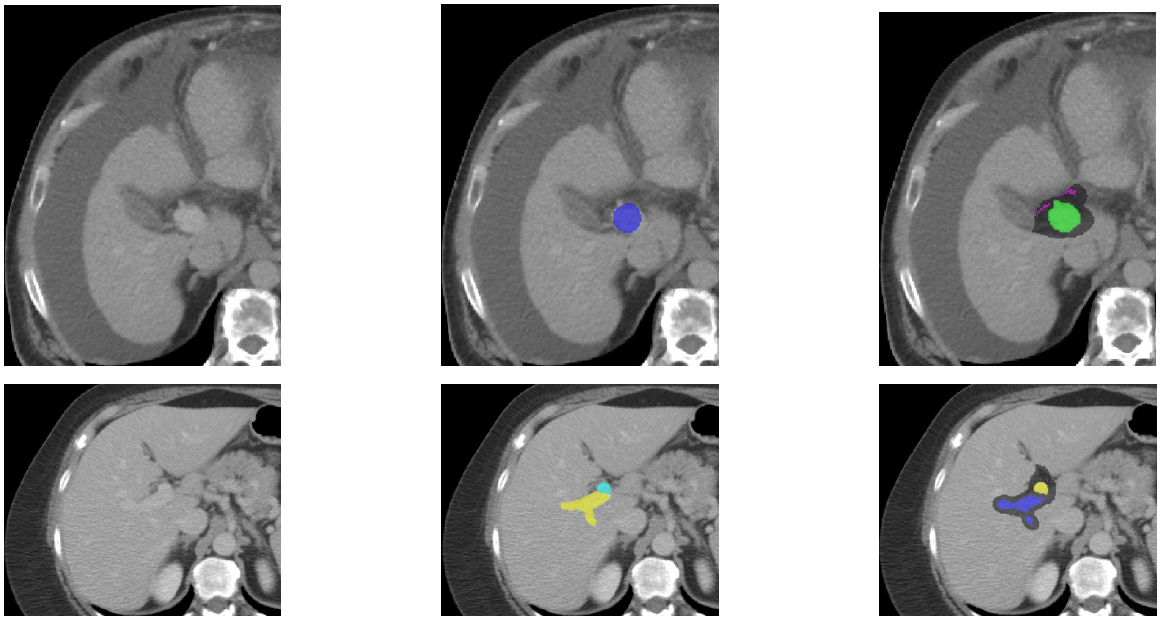

Figure 2: Top row is for a cirrhotic patient with ascites, and bottom row is for a normal patient. Last column shows the predicted segmentations of the main portal vein (green), right branch (blue) and left branch (yellow). The perivascular region (dark gray) was extracted and PVAT voxels (magenta) in the [-190, -30] range were identified.

2.5. Statistical Analysis

Dice similarity coefficient (DSC) and Hausdorff Distance (HD) error was used to assess the portal vein segmentation in 25 UW CT volumes. Several uni- and multi-variate logistic regression models were built (LR, scikit-learn package, Python v3.12) to diagnose fibrosis stages (advanced fibrosis group included cirrhosis patients). The UW dataset was divided into training (80%, n = 385 patients) and testing (20%, n = 95 patients) subsets. The test data subset contained 19 randomly sampled patients from each fibrosis stage.

Regression analysis was conducted following the same approach as prior work (Tallam et al., 2022). The models used various combinations of the serum (APRI and FIB-4 scores) and automated CT biomarkers as features. For the univariate analysis, multinomial logistic regression models were created for each of the 33 features separately. For the multivariate analysis, a stepwise approach determined the optimal set of explanatory features. Adjustment for multiple comparisons was not done. Instead, a general rule-of-thumb p-value threshold of 0.0015 (0.05/33) was used to identify the best features for final modeling.

For the model with the best features, a further sub-analysis was conducted. Three other models were created from the best model: (1) without both serum and PVAT features, (2) with serum but without PVAT features, and (3) without serum but with PVAT features, respectively. Performance was assessed with AUC (and 95% confidence intervals), sensitivity, and specificity. A model with an AUC above 0.6 was considered effective. A

Table 1: Results of portal vein segmentation by 3D nnU-Net on the UW dataset. PV: Portal Vein. DSC: Dice Score. HD: Hausdorff Distance error in mm.

Structure	DSC (%) ↑	HD (mm) ↓
Main PV	85.8 ± 10.2 (IQR: 82.8, 92.3)	3.0 ± 2.4 (IQR: 1.6, 3.1)
Left PV	81.4 ± 12.8 (IQR: 76.8, 92.0)	7.1 ± 6.9 (IQR: 3.3, 8.4)
Right PV	82.5 ± 14.6 (IQR: 76.7, 94.6)	7.9 ± 8.7 (IQR: 0.8, 9.9)
Full PV	86.4 ± 9.6 (IQR: 80.3, 92.9)	6.9 ± 7.1 (IQR: 2.4, 9.0)

bootstrapped DeLong test (MLstatkit package, Python v.3.12) compared the ROC curves from two models. A p-value < 0.05 was considered statistically significant.

3. Results

3.1. Portal Vein Segmentation

Table 1 and Fig. 2 show the 3D nnU-Net segmentation performance for delineating the portal vein and its branches (left and right). The model segmented the main portal vein branch with a DSC of 85.8 ± 10.2 and HD error of 3.0 ± 2.4 mm. Compared to the main branch, higher HD errors were seen for the left branch (7.1 ± 6.9 mm) and right branch (7.9 ± 8.7 mm), respectively. Segmentation of the full portal vein (combination of main and all branches) was satisfactory with a DSC of 86.4 ± 9.6 and HD error of 6.9 ± 7.1 mm.

3.2. Univariate Results

Table 2 shows the results from the univariate models. For cirrhosis, FIB-4 score obtained an AUC of 88.5% and specificity of 89.5%, but the sensitivity was lower at 73.7%. Among the CT features, spleen volume yielded the highest AUC of 89.2% and specificity of 94.7%. The SD of normalized CT attenuation for the right portal vein was the best PVAT feature with an AUC of 79.6%. For advanced fibrosis, FIB-4 score and spleen volume achieved the highest AUCs among the serum and CT imaging features, respectively. However, AUC for the SD of normalized CT attenuation for the main portal vein was the highest at 67.1%.

3.3. Multivariate Results

Table 2 also provides the multivariate modeling results. Figure 3 shows ROC curves of the different multi-variate models for advanced fibrosis and cirrhosis.

Cirrhosis: The best CT imaging features for predicting cirrhosis (without serum or PVAT scores) included the LSVR, LSN, spleen volume, and volume proportions of Couinaud segments except segment 7. This was the "baseline" model. It achieved a 91.6% AUC and 97.4% specificity. Adding serum scores slightly improved the AUC by 0.2%, but specificity dropped by 1%. Adding PVAT biomarkers to the baseline model resulted in a small AUC increase to 92.9%. However, the specificity fell to 90.8%. The PVAT biomarkers that were predictive included: (1) normalized SD CT attenuation for the main, left, and right portal veins, and (2) fat volume at the right portal vein. Adding both serum and PVAT features improved the baseline AUC to 93.3% with a specificity of 93.4%. The sensitivity of

Table 2: Results from the uni- and multi-variate logistic regression models with 95% confidence intervals. Blood serum scores (FIB-4 and APRI), Liver Surface Nodularity (LSN), Portal Vein (PV), Perivascular Adipose Tissue (PVAT), standard deviation (SD) of normalized (Norm) CT attenuation (Att).

	Advanced Fibrosis			Cirrhosis		
	AUC	Sensitivity	Specificity	AUC	Sensitivity	Specificity
FIB4	83.2 (74.1, 91.6)	68.4 (52.6, 82.9)	86.0 (75.4, 94.6)	88.5 (78.0, 96.7)	73.7 (50.0, 91.7)	89.5 (82.2, 95.8)
APRI	73.8 (62.0, 84.1)	52.6 (35.5, 68.4)	87.7 (78.0, 94.9)	82.3 (68.9, 93.0)	73.7 (53.3, 93.3)	84.2 (75.6, 92.0)
Spleen Volume	82.0 (71.7, 90.9)	71.1 (56.5, 84.6)	82.5 (71.2, 91.4)	89.2 (77.1, 98.3)	73.7 (53.3, 93.4)	94.7 (88.9, 98.8)
LSN	76.3 (64.8, 86.7)	65.8 (50.0, 79.5)	80.7 (70.2, 91.2)	88.1 (79.9, 95.1)	78.9 (57.7, 94.7)	88.2 (80.3, 94.9)
Main PV PVAT SD Norm. Att.	67.1 (55.6, 77.4)	50.0 (34.9, 65.8)	77.2 (65.5, 88.0)	70.3 (56.3, 83.1)	63.2 (41.7, 84.6)	68.4 (57.5, 78.5)
Right PV PVAT SD Norm. Att.	64.5 (53.1, 74.6)	78.9 (65.7, 91.2)	49.1 (35.7, 61.7)	79.6 (69.0, 88.6)	94.7 (83.3, 100.0)	53.9 (42.3, 64.6)
Baseline	84.8 (75.9, 92.2)	68.4 (53.3, 83.3)	87.7 (77.8, 95.3)	91.6 (82.0, 98.5)	73.7 (53.3, 93.4)	97.4 (93.2, 100.0)
Baseline & Serum	88.5 (81.0, 94.8)	86.8 (75.0, 97.1)	73.7 (61.4, 84.6)	91.8 (83.5, 98.4)	78.9 (57.9, 95.9)	96.1 (91.0, 100.0)
Baseline & PVAT	83.2 (74.3, 90.8)	55.3 (37.8, 71.0)	94.7 (88.6, 100.0)	92.9 (86.5, 98.1)	78.9 (58.8, 95.2)	90.8 (84.0, 96.3)
baseline & Serum & PVAT	88.7 (81.2, 94.7)	84.2 (72.5, 94.6)	73.7 (62.3, 85.4)	93.3 (86.5, 98.5)	78.9 (57.9, 94.7)	93.4 (87.3, 98.7)

this model was the highest at 78.9%. All multivariate models were significantly different ($p < .05$) from APRI score, and normalized mean and SD CT attenuation for main and right portal vein. However, statistical testing showed no difference between the multivariate models.

Advanced Fibrosis: The best CT imaging features for predicting advanced fibrosis were the same features from predicting Cirrhosis (see above). The baseline model attained 84.8% AUC and 87.7% specificity. Addition of the serum scores improved the AUC by ∼4%, but the specificity reduced to 73.7%. Addition of the PVAT features reduced the AUC to 83.2% and sensitivity to 55.3%, but the specificity was the highest at 94.7%. The PVAT scores included the normalized SD CT attenuation for the main, left, and right portal veins, respectively. Finally, inclusion of both PVAT and serum features to the baseline model led to the highest AUC of 88.7%, sensitivity of 84.2%, and specificity of 73.7%. This multivariate model was significantly different ($p < .05$) from all univariate models except FIB4 score and spleen volume. Again, statistical testing showed no difference between the various multivariate models.

4. Discussion

The main contributions in this work included: (1) automated fine-grained segmentations of the portal vein and its branches (left and right), and (2) use of a novel PVAT CT biomarker for staging fibrosis. A DSC score of 86.4 ± 9.6 was obtained for the segmentation of the portal vein. Our results are similar to those obtained by prior approaches (Li et al., 2024; Ibragimov et al., 2017), wherein DSC scores of 70% - 89% were achieved. As a result, the portal vein segmentation by the 3D nnU-Net model was deemed satisfactory for clinical use.

With the serum and PVAT biomarkers, multivariate models were trained to achieve AUCs of 91% - 93.5% and 83% - 89% for cirrhosis and advanced fibrosis, respectively. In prior literature by Lee et al. (2022) on the same UW dataset, AUCs of 94% and 80% were obtained for diagnosing cirrhosis and advanced fibrosis, respectively. Similarly, Lewis et al. (2024) obtained AUCs of 92.5% and 83.8% for cirrhosis and advanced fibrosis, respectively. The latter approach also used explainable biomarkers for staging hepatic fibrosis, such as

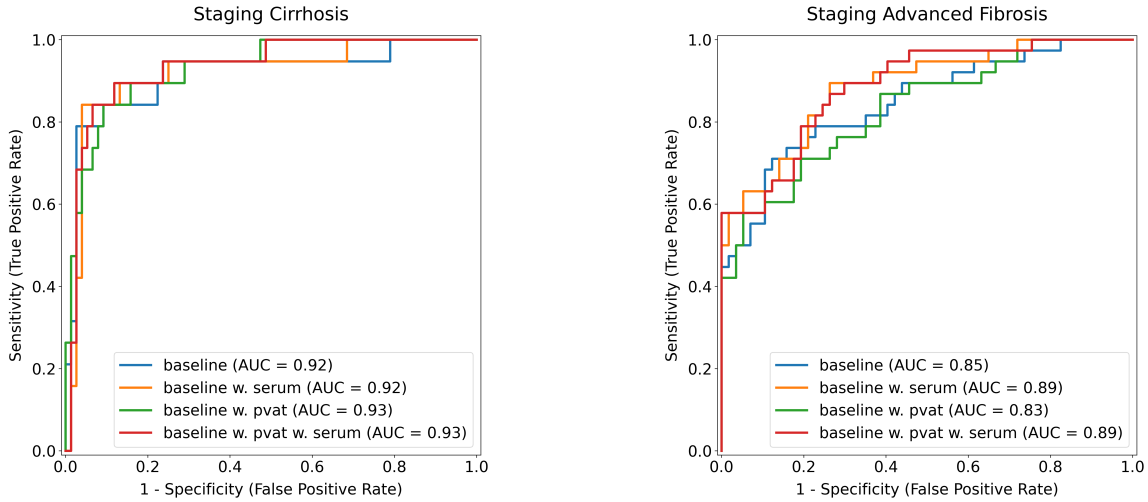

Figure 3: ROC curves for staging cirrhosis (left) and advanced fibrosis (right) with logistic regression models.

spleen volume, LSVR, and LSN. Other works (Choi et al., 2018) utilized neural networks to directly diagnose the fibrosis. AUCs of 0.97 and 0.95 were achieved for advanced fibrosis and cirrhosis, respectively. However, this approach required a large proprietary dataset of >7000 patients, rendering it challenging to replicate due to a lack of publicly available datasets with a large number of patients and confirmed fibrosis stages.

Limitations of this work are acknowledged. First, the PVAT biomarkers were not very predictive on their own for advanced fibrosis or cirrhosis. This may be attributed to the underlying patient pathophysiology. For example, upon a qualitative analysis, eight patients amongst the 19 cirrhotic patients in the UW test dataset had ascites (fluid buildup in the abdomen). From Fig. 2, ascites masked the visceral fat in the periportal region, appeared brighter than the CT attenuation range of [-190, -30] for fat, and fewer PVAT voxels were identified as a result. The predictive value of PVAT biomarkers increased when combined with other features, such as serum or other CT imaging biomarkers (e.g., spleen volume). Next, periportal space widening may be more pronounced in certain patients in contrast to others, such as lean individuals with lower BMI (Ludwig et al., 2021). Based on this evidence, the clinical utility of using PVAT features is questionable. As there is scant research on automated techniques to measure periportal fat (Song et al., 2024; Ludwig et al., 2021; Ito et al., 2000), our findings hold value for furthering research into hepatic PVAT. Second, PVAT biomarkers were not extracted from the hepatic arteries and hepatic veins in this work. The diagnostic performance may improve with their incorporation. Third, the automated approach was not validated on non-contrast CT. Lastly, the sample size used in this work was small (19 patients from each fibrosis stage). External validation on additional patients is necessary to further clarify the findings. This is the subject of future work.

In summary, the non-invasive imaging-based biomarkers PVAT derived in this work were useful for staging advanced fibrosis and cirrhosis. The current approach shows promise for population-based studies of metabolic disease and opportunistic screening.

Acknowledgments

This work was supported by the Intramural Research Program of the NIH Clinical Center (project number 1Z01 CL040004). The research used the high-performance computing facilities of the NIH Biowulf cluster.

References

American Liver Foundation. Fibrosis: Development, June 2022. URL https://liverfoundation.org/about-your-liver/how-liver-diseases-progress/fibrosis-scarring/. Accessed: 2024-08-05.

M. Antonelli, A. Reinke, et al. The medical segmentation decathlon. *Nat Commun*, 13(1): 4128, 2022.

Centers for Disease Control and Prevention. Chronic Liver Disease, April 2024. URL https://www.cdc.gov/nchs/fastats/liver-disease.htm. Accessed: 2024-08-05.

Devina Chatterjee, Benjamin L. Shou, Matthew B. Matheson, Mohammad R. Ostovaneh, Carlos Rochitte, Marcus Y. Chen, Marc Dewey, Jason Ortman, Christopher Cox, Joao A.C. Lima, and Armin Arbab-Zadeh. Perivascular fat attenuation for predicting adverse cardiac events in stable patients undergoing invasive coronary angiography. *Journal of Cardiovascular Computed Tomography*, 16(6):483–490, 2022. ISSN 1934-5925. doi: https://doi.org/10.1016/j.jcct.2022.05.004. URL https://www.sciencedirect.com/science/article/pii/S1934592522000727.

Kyu Jin Choi, Jong Keon Jang, Seung Soo Lee, Yu Sub Sung, Woo Hyun Shim, Ho Sung Kim, Jessica Yun, Jin-Young Choi, Yedaun Lee, Bo-Kyeong Kang, Jin Hee Kim, So Yeon Kim, and Eun Sil Yu. Development and validation of a deep learning system for staging liver fibrosis by using contrast agent–enhanced ct images in the liver. *Radiology*, 289 (3):688–697, 2018. doi: 10.1148/radiol.2018180763. URL https://doi.org/10.1148/radiol.2018180763. PMID: 30179104.

Bulat Ibragimov, Diego Toesca, Daniel Chang, Albert Koong, and Lei Xing. Combining deep learning with anatomical analysis for segmentation of the portal vein for liver sbrt planning. *Physics in Medicine & Biology*, 62(23):8943, nov 2017. doi: 10.1088/1361-6560/aa9262. URL https://dx.doi.org/10.1088/1361-6560/aa9262.

Fabian Isensee, Paul F Jaeger, Simon AA Kohl, Jens Petersen, and Klaus H Maier-Hein. nnu-net: a self-configuring method for deep learning-based biomedical image segmentation. *Nature methods*, 18(2):203–211, 2021.

Fabian Isensee et al. nnu-net revisited: A call for rigorous validation in 3d medical image segmentation. *ArXiv*, abs/2404.09556, 2024. URL https://api.semanticscholar.org/CorpusID:269148560.

Katsuyoshi Ito, Donald G. Mitchell, and Toshifumi Gabata. Enlargement of hilar periportal space: A sign of early cirrhosis at mr imaging. *Journal of Magnetic Resonance Imaging*, 11(2):136–140, 2000. doi: https://doi.org/10.1002/(SICI)1522-2586(200002)11:2⟨136::

AID-JMRI9⟩3.0.CO;2-B. URL https://onlinelibrary.wiley.com/doi/abs/10.1002/%28SICI%291522-2586%28200002%2911%3A2%3C136%3A%3AAID-JMRI9%3E3.0.CO%3B2-B.

Darcy E. Kahn and Bryan C. Bergman. Keeping it local in metabolic disease: Adipose tissue paracrine signaling and insulin resistance. *Diabetes*, 71(4):599–609, 03 2022. ISSN 0012-1797. doi: 10.2337/dbi21-0020. URL https://doi.org/10.2337/dbi21-0020.

Musturay Karcaaltincaba, Mithat Haliloglu, Erhan Akpinar, Deniz Akata, Mustafa Ozmen, Macit Ariyurek, and Okan Akhan. Multidetector ct and mri findings in periportal space pathologies. *European Journal of Radiology*, 61(1):3–10, 2007. ISSN 0720-048X. doi: https://doi.org/10.1016/j.ejrad.2006.11.009. URL https://www.sciencedirect.com/science/article/pii/S0720048X06004499. Diffuse Liver Diseases.

Guido Lastra and Camila Manrique. Perivascular adipose tissue, inflammation and insulin resistance: link to vascular dysfunction and cardiovascular disease. *Hormone Molecular Biology and Clinical Investigation*, 22(1):19–26, 2015. doi: doi:10.1515/hmbci-2015-0010. URL https://doi.org/10.1515/hmbci-2015-0010.

S. Lee, D. C. Elton, A. H. Yang, et al. Fully Automated and Explainable Liver Segmental Volume Ratio and Spleen Segmentation at CT for Diagnosing Cirrhosis. *Radiology: Artificial Intelligence*, 4(5):e210268, 2022. doi: 10.1148/ryai.210268.

Sydney V. Lewis, Tejas S. Mathai, Meghan G. Lubner, Perry J. Pickhardt, and Ronald M. Summers. Utility of Fully Automated Liver and Spleen Biomarkers for Staging Hepatic Fibrosis in CT. *Scientific Abstracts from the 2024 Conference on Machine Intelligence in Medical Imaging (CMIMI) of the Society for Imaging Informatics in Medicine (SIIM), Journal of Imaging Informatics in Medicine (Supplement)*, 37(1):1–35, 2024.

Shengwei Li, Xiao-Guang Li, Fanyu Zhou, Yumeng Zhang, Zhixin Bie, Lin Cheng, Jinzhao Peng, and Bin Li. Automated segmentation of liver and hepatic vessels on portal venous phase computed tomography images using a deep learning algorithm. *Journal of Applied Clinical Medical Physics*, 25(8):e14397, 2024. doi: https://doi.org/10.1002/acm2.14397. URL https://aapm.onlinelibrary.wiley.com/doi/abs/10.1002/acm2.14397.

Daniel R. Ludwig, Tyler J. Fraum, David H. Ballard, Vamsi R. Narra, and Anup S. Shetty. Imaging biomarkers of hepatic fibrosis: Reliability and accuracy of hepatic periportal space widening and other morphologic features on mri. *American Journal of Roentgenology*, 216(5):1229–1239, 2021. doi: 10.2214/AJR.20.23099. PMID: 33729883.

Tejas S. Mathai, Meghan G. Lubner, Perry J. Pickhardt, and Ronald M. Summers. Fully Automated and Explainable Measurement of Liver Surface Nodularity in CT: Utility for Staging Hepatic Fibrosis . *Academic Radiology*, 1(1):1–10, 2024a.

Tejas S. Mathai et al. Liver Surface Nodularity for Staging Hepatic Fibrosis on CT: A Comparative Study of Liver Segmenters. *Scientific Abstracts from the 2024 Conference on Machine Intelligence in Medical Imaging (CMIMI) of the Society for Imaging Informatics in Medicine (SIIM), Journal of Imaging Informatics in Medicine (Supplement)*, 37(1):1–35, 2024b.

N R. Mazumder, B. Enchakalody, P. Zhang, and G.L. Su. Using Artificial Intelligence to Predict Cirrhosis From Computed Tomography Scans. *Clinical and Translational Gastroenterology*, 14(10), 2023. doi: 10.14309/ctg.0000000000000616.

Andrew M. Nguyen, Tejas Sudharshan Mathai, Liangchen Liu, Jianfei Liu, and Ronald M. Summers. Automated measurement of pericoronary adipose tissue attenuation and volume in ct angiography. In *2024 IEEE International Symposium on Biomedical Imaging (ISBI)*, pages 1–5, 2024. doi: 10.1109/ISBI56570.2024.10635570.

P. J. Pickhardt, K. Malecki, J. Kloke, and M. G. Lubner. Accuracy of Liver Surface Nodularity Quantification on MDCT as a Noninvasive Biomarker for Staging Hepatic Fibrosis. *American Journal of Roentgenology*, 207(6):1194–1199, 2016. doi: 10.2214/AJR.16.16514.

P. J. Pickhardt, K. Malecki, C. Beaumont O.F. Hunt, J. Kloke, T.J. Ziemlewicz, and M. G. Lubner. Hepatosplenic volumetric assessment at MDCT for staging liver fibrosis. *European Radiology*, 27:3060–3068, 2017. doi: 10.1007/s00330-016-4648-0.

Bin Song, Yali Qu, Jie Chen, Jie Yang, Hua-Lin Yan, Han-Yu Jiang, and Bin Song. Noninvasive diagnosis of liver cirrhosis: qualitative and quantitative imaging biomarkers. *Abdominal Radiology*, feb 2024. doi: 10.1007/s00261-024-04225-8. URL https://doi.org/10.1007/s00261-024-04225-8.

Hima Tallam et al. Fully Automated Abdominal CT Biomarkers for Type 2 Diabetes Using Deep Learning. *Radiology*, 304(1):85–95, 2022. doi: 10.1148/radiol.211914. URL https://doi.org/10.1148/radiol.211914. PMID: 35380492.

Alessia Valentini, Carmine Cardillo, David Della Morte, and Manfredi Tesauro. The role of perivascular adipose tissue in the pathogenesis of endothelial dysfunction in cardiovascular diseases and type 2 diabetes mellitus. *Biomedicines*, 11(11), 2023. ISSN 2227-9059. doi: 10.3390/biomedicines11113006. URL https://www.mdpi.com/2227-9059/11/11/3006.

Jakob Wasserthal, Hanns-Christian Breit, Manfred T Meyer, Maurice Pradella, Daniel Hinck, Alexander W Sauter, Tobias Heye, Daniel T Boll, Joshy Cyriac, Shan Yang, et al. Totalsegmentator: robust segmentation of 104 anatomic structures in ct images. *Radiology: Artificial Intelligence*, 5(5), 2023.

Y. Yin, D. Yakar, R. A. J. O. Dierckx, K. B. Mouridsen, T. C. Kwee, and R. J. de Haas. Liver fibrosis staging by deep learning: a visual-based explanation of diagnostic decisions of the model. *European Radiology*, 31(12):9620–9627, 2021. doi: 10.1007/s00330-021-08046-x.

Harvey A. Ziessman, Janis P. O'Malley, and James H. Thrall. Chapter 7 - hepatobiliary system. In Harvey A. Ziessman, Janis P. O'Malley, and James H. Thrall, editors, *Nuclear Medicine (Third Edition)*, The Requisites in Radiology, pages 159–214. Mosby, Philadelphia, third edition edition, 2006. ISBN 978-0-323-02946-9. doi: https://doi.org/10.1016/B978-0-323-02946-9.50012-X. URL https://www.sciencedirect.com/science/article/pii/B978032302946950012X.